Carbohydrate Polymers 90 (2012) 1601–1608

Contents lists available at SciVerse ScienceDirect

Carbohydrate Polymers

journal homepage: www.elsevier.com/locate/carbpol

Mechanical and barrier properties of nanocrystalline cellulose reinforced chitosan based nanocomposite films

Avik Khan [a], Ruhul A. Khan [a], Stephane Salmieri [a], Canh Le Tien [a], Bernard Riedl [b], Jean Bouchard [c], Gregory Chauve [c], Victor Tan [d], Musa R. Kamal [d], Monique Lacroix [a,*]

[a] Research Laboratories in Sciences Applied to Food, Canadian Irradiation Centre (CIC), INRS-Institute Armand-Frappier, University of Quebec, 531 Boulevard des Prairies, Laval, Quebec H7V 1B7, Canada
[b] Département des sciences du bois et de la forêt, Faculté de foresterie, géographie et géomatique, Université Laval, Quebec-city, Quebec G1V 0A6, Canada
[c] FPInnovations, 570 Boulevard St. Jean, Pointe-Claire, Quebec H9R 3J9, Canada
[d] Department of Chemical Engineering, McGill University, 3610 University Street, Montreal, QC H3A 2B2, Canada

ARTICLE INFO

Article history:
Received 30 April 2012
Received in revised form 22 June 2012
Accepted 9 July 2012
Available online 16 July 2012

Keywords:
Chitosan
Nanocrystalline cellulose
Biodegradable
Nanocomposite films
Mechanical properties
Barrier properties

ABSTRACT

Nanocrystalline cellulose (NCC) reinforced chitosan-based biodegradable films were prepared by solution casting. The NCC content in the films was varied from 1 to 10% (dry wt. basis). It was found that the tensile strength (TS) of the nanocomposite films with 5% (w/w) NCC content was optimum with an improvement of 26% compared to the control chitosan films. Incorporation of NCC also significantly improved barrier properties. Water vapor permeability (WVP) of the chitosan/NCC films was decreased by 27% for the optimum 5% (w/w) NCC content. Swelling studies revealed a decrease in water uptake of the NCC-reinforced chitosan films. Analyses of thermal properties showed no significant effect of NCC whereas X-ray diffraction studies confirmed the appearance of crystalline peaks in the nanocomposite films. Surface morphology of the films was investigated by scanning electron microscopy and it was found that NCC was dispersed homogenously into chitosan matrix.

1. Introduction

Global environmental concern, regarding the use of non-biodegradable petroleum-based packaging materials, has been encouraging researchers, industries and governments in the quest for alternative materials made from natural biopolymers. Bio-based packaging is made from raw materials originating from natural sources, such as starch, cellulose, chitin or biodegradable synthetic polymers such as, polycaprolactone and polylactic acid (Arumugam, Tamareselvy, Venkata Rao, & Rajalingam, 1989; Chandra & Rustgi, 1998; Ciesla, Salmieri, & Lacroix, 2006; Le Tien et al., 2000). Despite great improvements, the use of natural polymers for food packaging has been limited because of the poor barrier properties and weak mechanical properties of the film (Rhim & Perry, 2007). For these reasons natural polymers were either blended with other synthetic polymers or chemically modified to enhance these features (Giannelis, 1996; Khan, Huq, et al., 2010; Weber, Haugaard, Festersen, & Bertelsen, 2002). Some of the limited mechanical and barrier properties (water vapor, oxygen permeability, etc.) of biopolymers can be significantly enhanced by the use of reinforcing fillers to create nanocomposite films. Nanocomposite films extend the food shelf-life, and also improve food quality as they can serve as carriers of some active substances, such as antioxidants and antimicrobials (Sorrentino & Gorrasi, 2007).

Chitosan, a natural linear polysaccharide consisting of 1,4-linked 2-amino-deoxy-β-D-glucan, is a partially deacetylated derivative of chitin, the second most abundant natural polysaccharide after cellulose. Chitosan is non-toxic, biodegradable, biofunctional, biocompatible and was reported by several researchers to have strong antimicrobial and antifungal activities (Darmadji & Izumimoto, 1994; Kim et al., 2011; No, Meyers, Prinyawiwatkul, & Xu, 2007; Rabea, Badawy, Stevens, Smagghe, & Steurbaut, 2003). Chitosan films have been successfully used as a packaging material for the quality of preservation of foods (Jo, Lee, Lee, & Byun, 2001).

Cellulose, another natural linear carbohydrate polymer chain consisting of D-glucopyranose units joined together by β-1,4-glycosidic linkages, is the most abundant biopolymer and can be found in wood, cotton, hemp among other sources. Cellulose nanocrystals, also called nanocrystalline cellulose (NCC) can be extracted from cellulose sources after the cellulose fibers are digested by a controlled acid hydrolysis process. NCC is a highly

* Corresponding author. Tel.: +1 450 687 5010; fax: +1 450 686 5501.
E-mail address: monique.lacroix@iaf.inrs.ca (M. Lacroix).

0144-8617/$ – see front matter © 2012 Elsevier Ltd. All rights reserved.
http://dx.doi.org/10.1016/j.carbpol.2012.07.037

crystalline nanometer sized rod-like particle that is obtained as a stable aqueous colloidal suspension. This NCC was extracted from softwood bleached kraft pulp with an acid hydrolysis process inspired from the literature (Beck-Candanedo, Roman, & Gray, 2005). This type of NCC was found to exhibit an average length of 110 nm long for a 5–10 nm width (Revol, Bradford, Giasson, Marchessault, & Gray, 1992). The use of sulfuric acid in the hydrolysis process, leads to a more stable dispersion than the one using hydrochloric acid due to the grafting of sulfate groups on the surface of the NCC that stabilizes the NCC suspensions by electrostatic repulsion (Beck-Candanedo et al., 2005). NCC was shown to reinforce polymers due to the formation of a percolation network that connects the well dispersed NCC by hydrogen bonds (Favier, Chanzy, & Cavaille, 1996). It was shown that the presence of NCC reinforcing fillers in the polymer matrix provides superior performances such as mechanical properties, barrier properties leading to the next generation of biodegradable materials (Azeredo et al., 2010; Cao, Chen, Chang, Muir, & Falk, 2008; Dieter-Klemm et al., 2009).

The objective of the present research was to evaluate the effect of NCC incorporation on the mechanical, barrier, thermal and structural properties of chitosan-based biodegradable films. The mechanical properties of the films were measured to evaluate the films tensile strength (TS), tensile modulus (TM), and elongation at break (Eb). The barrier properties of the films were investigated by carrying out water vapor permeability tests and swelling properties were monitored by the water uptake of the nanocomposite films. Fourier Transform Infrared Spectroscopy (FTIR) was used analyze the interaction between chitosan and NCC. Surface morphology of the NCC reinforced chitosan films was investigated by scanning electron microscopy (SEM).

2. Materials and methods

2.1. Materials

Chitosan (high mol. weight, degree of deacetylation: 88–89%) was purchased from Kitomer Biotech (Rivière-au-Renard, QC, Canada). NCC (prepared as a dry redispersible powder in water) was produced in the FPInnovations pilot plant NCC reactor (Pointe-Claire, QC, Canada) from a commercial bleached softwood kraft pulp according to a procedure modified from the literature (Dong, Revol, & Gray, 1998).

2.2. Film preparation

Chitosan (1%, w/v) was dissolved in 2% aqueous acetic acid solution. A dilute aqueous NCC suspension (0.1%, w/w) was prepared by dispersing the NCC powder in distilled water for 3 h, under vigorous magnetic stirring at room temperature, followed by ultrasonication in a water bath for 30 min. The NCC suspension (1–10%, w/w in the dry chitosan-based nanocomposite film) was mixed with the chitosan solution and homogenized at 23,000 rpm for 2 min with a high shear mixer (IKA T25 digital Ultra-Turrax disperser, IKA Works Inc., Wilmington, NC, USA). Films were then cast by applying 10 mL of the NCC/chitosan suspension onto Petri dishes (100 mm × 15 mm) and air-dried for 24 h, at room temperature at 35% relative humidity (RH). Dried nanocomposite films were peeled off from the Petri dishes and stored in polyethylene bags at 35% RH prior to characterization. The thickness of the films was ~20 μm. Pure NCC films were prepared by casting from a 1% NCC suspension.

2.3. Mechanical properties of the films

Tensile strength (TS), tensile modulus (TM) and elongation at break (Eb) of the films were measured by using Universal Testing Machine (model H5KT, with a 1 kN load cell, Tinius-Olsen, Horsham, USA). The samples were cut using ASTM procedure D 638-99 and the film thickness was measured using a Mitutoyo Digimatic Indicator (Type ID-110E; Mitutoyo Manufacturing Co. Ltd., Tokyo, Japan) at five random positions along the film.

2.4. Water vapor permeability test

The WVP test was conducted gravimetrically using ASTM procedure 15.09:E96. Films were mechanically sealed onto Vapometer cells (No. 68-1, Twhing-Albert Instrument Co., West Berlin, NJ, USA) containing 30 g of anhydrous calcium chloride to create a 0% RH storage condition). The cells were initially weighed and placed in a Shellab 9010 L controlled humidity chamber (Sheldon Manufacturing Inc., Cornelius, OR, USA) maintained at 25 °C and 60% RH for 24 h, then the amount of water vapor transferred through the film and absorbed by the desiccant was determined from the weight gain of the cell. The assemblies were weighed initially and after 24 h for all samples. WVP is calculated according to the combined Fick and Henry's laws for gas diffusion through films as follows:

$$\mathrm{WVP(g\ mm/m^2\ day\ kPa)} = \frac{x\Delta w}{A\Delta P}$$

where Δw is the weight gain of the cell (g) after 24 h, x is the film thickness (mm), A is the area of exposed film ($31.67 \times 10^{-4}\ \mathrm{m^2}$), and ΔP is the differential vapor pressure of water through the film (ΔP = 3.282 kPa at 25 °C). WVP is expressed in g mm/m^2 day kPa.

2.5. Gel swelling property

The test samples were first dried at 37 °C for 12 h in an incubator and then accurately weighed. The dried films were then immersed in distilled water for 1–8 h. The wet weight of the films was measured by taking out the films from the water and blotting with a filter paper to remove the surface adsorbed water followed by immediately weighing the films (Jin, Song, & Hourston, 2004). The water uptake or swelling property of the films was calculated by the following equation:

$$S = \left[\frac{W_s - W_d}{W_d}\right] \times 100$$

where, S is the percentage of water absorption of the films at equilibrium; W_s and W_d are the weights (in g) of the samples in the dry and swollen states, respectively.

2.6. Fourier transform infrared spectroscopy (FTIR)

The FTIR spectra of the films were recorded using a Spectrum One spectrophotometer (Perkin-Elmer, Woodbridge, ON, Canada) equipped with an attenuated total reflectance (ATR) device for solids analysis and a high-linearity lithium tantalate detector. Spectra were analyzed using Spectrum 6.3.5 software. Films were stored at room temperature for 72 h in a desiccator containing saturated NaBr solution to ensure a stabilized atmosphere of 59% RH at 23 °C. Films were then placed onto a zinc selenide crystal, and the analysis was performed within the spectral region of 650–4000 cm^{-1} with 64 scans recorded at a 4 cm^{-1} resolution. After attenuation of total reflectance and baseline correction, spectra were normalized with a limit ordinate of 1.5 absorbance units.

2.7. Thermo gravimetric analysis (TGA)

Thermogravimetric analysis of the films was carried out using a TGA 7 (Perkin Elmer, CA, USA) analyser. Experiments were carried out under nitrogen atmosphere (40 cm L min^{-1}). The weight of the

film samples varied from 6 to 8 mg, scanning range was maintained to 50–600 °C and the heating rate was 10 °C min^{-1}.

2.8. X-ray diffraction (XRD)

For XRD analysis, film samples were folded several times to increase the sample thickness. Samples were analyzed between $2\theta = 5°$ and 30° with step increment $2\theta = 0.02°$ in a D8 Discover X-ray Diffractometer (Bruker AXS Inc., Madison, MI, USA) using a Cu Kα (40 kV/35 mA).

2.9. Scanning electron microscopy (SEM)

Film samples were prepared by dropping in liquid nitrogen a 5 mm × 5 mm sample piece that was previously cut from the center of the sample film. The sample piece was allowed to equilibrate in the liquid nitrogen prior to being fractured with a prechilled razor blade held in a vice grip. The samples were deposited on an aluminum holder and sputtered with gold/palladium alloy (deposition rate of 30 s equivalent to coating thickness of approximately 50 Å) in a Hummer IV sputter coater (Anatech Ltd, Alexandria, VA). SEM photographs were taken with a Hitachi S-4700 FEG-SEM (Hitachi Canada Ltd., Mississauga, ON, Canada) at a magnification of 40,000×, at room temperature. The microscope was equipped with an X-ray detector model 7200 (Oxford Instruments) with a resolution of 1.36 eV at 5.9 keV.

2.10. Statistical analysis

An analysis of variance (ANOVA) and multiple comparison tests of Duncan's were used to compare all the results. Differences between means were considered significant when the confidence interval is smaller than 5% ($P \leq 0.05$). The analysis was performed by the PASW Statistics 18 software (SPSS Inc., Chicago, IL, USA).

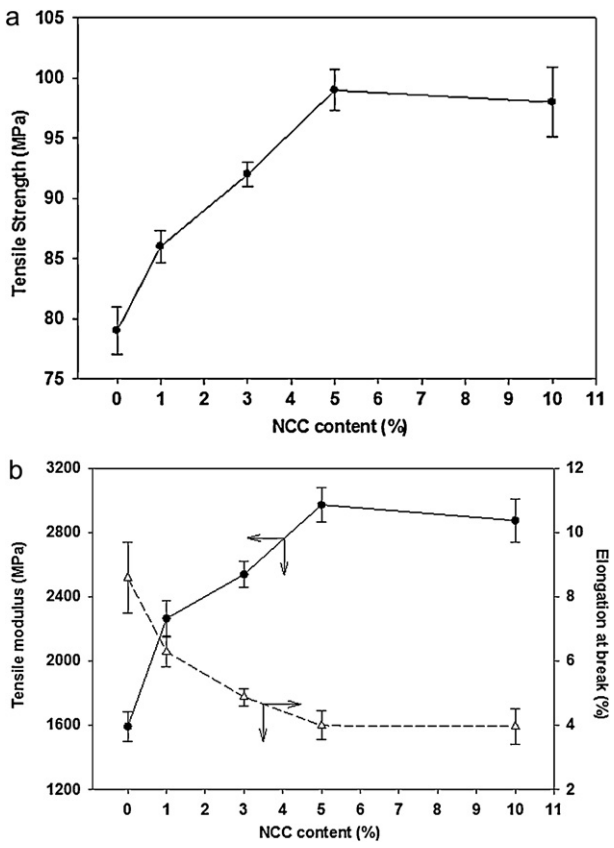

Fig. 1. (a) Effect of NCC content in the tensile strength of the chitosan films. (b) Effect of NCC content in the tensile modulus and elongation at break (%) of the chitosan films.

3. Results and discussion

3.1. Mechanical properties of the NCC reinforced chitosan-based films

The effect on the tensile strength of NCC incorporated in chitosan-based films was observed as a function of the NCC loading ranging between 1 and 10% (w/w) of the final dry weight of the film (Fig. 1a). The TS of pure chitosan films was found to be 79 MPa and the reinforced films with addition of 1, 3, 5 and 10% (w/w) NCC increased the TS values up to 86, 92, 99 and 98 MPa respectively ($P \leq 0.05$). The increase corresponds to a gain in TS of 8.8, 16.5, 25.3 and 24% compared to the control sample respectively. It turns out that the optimum NCC loading to get the best TS value ranges between 3 and 5% (w/w) after which the TS value tends to plateau. The increase in the TS values of the NCC-reinforced chitosan films can be attributed to two factors such as, (1) the favorable nanocrystal–polymer interactions and (2) the reinforcing effect occurred through effective stress transfer at the nanocrystal–polymer interface. The interaction between the anionic sulfate groups of NCC to the cationic amine groups of chitosan might favor a good interface between the matrix and the filler. This may lead to high TS values of the nanocomposite films (De Mesquita, Donnici, & Pereira, 2010). On the other hand, a mean field mechanical model may be adopted to explain the reinforcing effect of NCC observed in the current study. The mean-field model is based on the concept that the nanocrystals are homogeneously dispersed in the polymer matrix, but there is no interaction between the nanocrystals (Favier et al., 1996). The high mechanical strength of the nanocomposite films may results from efficient load transfer to the nanocrystal network, leading to more uniform stress distribution and minimization of the stress concentration area (Kanagaraj, Varanda, Zhil'tsova, Oliveira, & Simões, 2007). Beyond 5% (w/w) NCC, the TS values plateau suggesting that the addition of more NCC above this threshold concentration does not help to improve the TS. The reason for the value to plateau may be due to the potential aggregation of NCC particles after a certain concentration is reached, which results in no further improvement of mechanical properties. Li, Zhou, and Zhang (2009) reported excellent reinforcing properties of the cellulose nanocrystals and obtained almost a 41% increase in the TS of the chitosan films due to the incorporation of 15–20% (w/w) nanocrystals. The cellulose nanocrystal length and width reported in this manuscript was 400 nm in length and 24 nm in width, which is almost 4 times longer than the NCC used in the current study. This could be the reason why such a high nanocrystal loading (15–20%, w/w) was required to reach the percolation threshold and reinforce chitosan. Jalal Uddin, Araki, and Yasuo Gotoh (2011) reported the fabrication of polyvinyl alcohol (PVOH) nanocomposites reinforced with varying concentrations of cellulosic nanocrystals (0–30%, w/w) and have found that 5% (w/w) nanocrystal concentration is the optimum in terms of mechanical strength. Incorporation of cellulose nanocrystals also improved the mechanical strength of alginate nanocomposite fibers (Ureña-Benavides, Brown, & Kitchens, 2010). Fig. 1b shows the effect of the NCC content on the TM and Eb (%) of NCC-reinforced chitosan films. The TM value of the pure chitosan film was found to be 1590 MPa. The incorporation of 1% NCC caused a significant ($P \leq 0.05$) increase of TM (2264 MPa), which is an increase of more than 43% than the control chitosan films. At 5% NCC content, the TM value was found to be 2971 MPa, which corresponds to an increase of 87% compared to pure chitosan films. After 5%, the TM values of the films reach a plateau similar to the TS values as

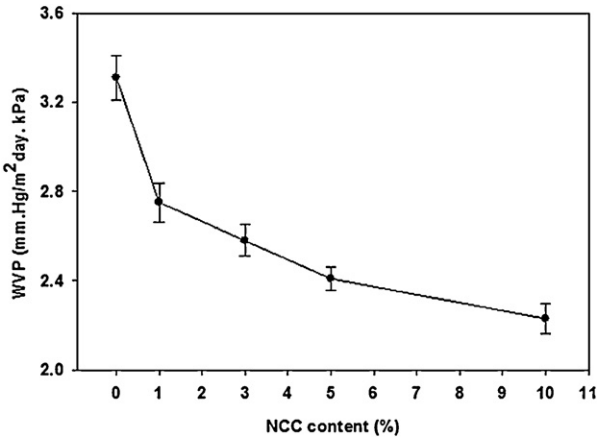

Fig. 2. Effect of NCC content in the water vapor permeability of the chitosan films.

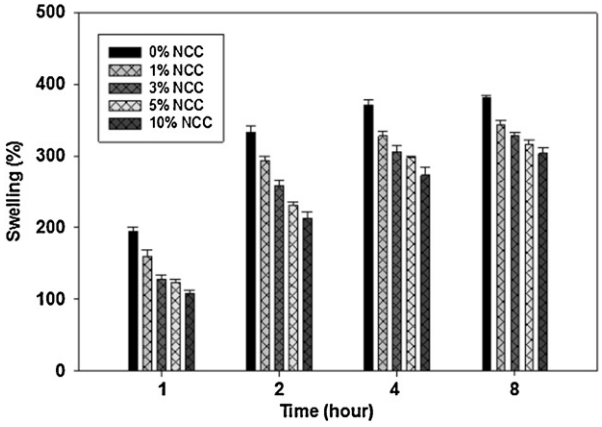

Fig. 3. Effect of NCC content in the swelling property of the chitosan films.

reported above. Filler-reinforced films usually tend to become more brittle as the concentration of the reinforcing particles increases (Cyras, Manfredi, Ton-That, & Vázquez, 2008; Lee et al., 2004; Rhim, 2011). This behavior is also common for nanocomposite films. The increased TM values of the NCC reinforced chitosan films may be attributed to the increased stiffness of the films by the addition of NCC. Ureña-Benavides et al. (2010) reported 123% increase in the TM of the calcium alginate fibers due to the incorporation of 10% (w/w) cellulose nanocrystals. Azeredo et al. (2009) and Jalal Uddin et al. (2011) have also reported an increase of TM values due to the addition of cellulose nanocrystals. Thus, NCC particles acted as a good reinforcing agent in chitosan films. The Eb value was found to be 8.58% for the pure chitosan film and 6.28, 4.87, 3.98 and 3.95 for 1, 3, 5 and 10% (w/w) of NCC addition respectively. After 5% NCC incorporation, the Eb values tend to a plateau which follows the similar trend as the TM values. Li et al. (2009) also observed a decrease in the Eb values of chitosan films from 20 to 6% due to the incorporation of cellulose nanocrystals. Such a decrease in Eb values indicated that the incorporation of NCC into the chitosan matrix resulted in strong interactions between filler and matrix, which restricted the motion of the matrix and hence decreased Eb (Azeredo et al., 2010; Azizi Samir, Alloin, Sanchez, & Dufresne, 2004).

3.2. Water vapor permeability

The effect of NCC concentration on the WVP of the chitosan films is illustrated in Fig. 2. The values of WVP decreased with the increase in NCC content, from 3.31 g mm/m^2 day kPa for the pure chitosan film down to 2.23 g mm/m^2 day kPa for the 10% loading of NCC. It is clearly observed that NCC had a great impact on the reduction of WVP values of chitosan-based films. The presence of cellulose nanocrystals is thought to increase the tortuosity in the chitosan films leading to slower water vapor diffusion processes and hence, to a lower permeability (Azeredo et al., 2010). Water vapor more favorably diffuses through the amorphous areas of the polymer matrix, so the degree of crystallinity is also of importance in the permeability behavior of the nanocomposite (Rhim, Hong, Park, & Ng, 2006). Azeredo et al. (2009) reported that the WVP of mango puree films improved significantly with the addition of cellulose nanocrystals. Paralikar, Simonsen, and Lombardi (2008) have also reported reduction in the WVP of PVOH films due to the addition of 10% (w/w) cellulose nanocrystals.

3.3. Gel swelling property

Fig. 3 illustrates the effect of NCC incorporation on the swelling percentages that corresponds to the water uptake of chitosan films. Presence of NCC significantly reduced the swelling percentage (S), of chitosan films. After 1 h, the S value of the pure chitosan films increased to 195%, whereas the S values of the nanocomposite films were only 123 and 108%, for 5 and 10% NCC, respectively. It was also observed that the S values of the NCC reinforced nanocomposite films (10% NCC) decreased again by 20% after 8 h of immersion in water as compared to the control chitosan film. In the above paragraph, it is reported that WVP of chitosan films were reduced because of the addition of NCC in chitosan films, which is in agreement with a decrease in the water uptake of NCC-containing chitosan films. Water uptake of the nanocomposite films depends on the nature of the matrix and filler. This phenomenon of decreased water uptake at equilibrium can be ascribed to the fact that highly crystalline NCC is less hydrophilic than chitosan and the formation of strong filler–matrix interactions (Dufresne, Dupeyre, & Vignon, 2000; Li et al., 2009). In the current study, the cellulose nanocrystals acted as an interpenetrated network within the matrix and prevented the swelling of the chitosan films when exposed to water. Dufresne et al. (2000) and Svagan, Hedenqvist, and Berglund (2009) have also reported similar decrease in water uptake of the nanocomposite films due to the addition of cellulose nanocrystals.

3.4. Fourier transform infrared spectroscopy

FTIR analysis attempted to characterize the effect of NCC incorporation on the chitosan films and to determine the infrared bands and shifts related to NCC–chitosan interactions. The position of the peaks of chitosan film spectrum is similar to those described by different authors (Cao, Dong, & Li, 2007; Chen et al., 2003; Sionkowska, Wisniewski, Skopinska, Kennedy, & Wess, 2004; Wu, Zivanovic, Draughon, Conway, & Sams, 2005). The absorption peaks of the chitosan films (Fig. 4a) are mainly assignable to the stretching of intra- and intermolecular O—H and —CH_2OH vibrations at 3500–3250, overlapped with stretching —NH_2 (3500–3400 cm^{-1}) and —NH secondary amides vibrations (3300–3280 cm^{-1}). Also 2960–2870 cm^{-1} corresponds to symmetric and asymmetric C—H vibrations. Amide I vibrational mode at 1633 cm^{-1} and amide II at 1538 cm^{-1} have also been observed. In the FTIR spectra of pure NCC films the broad absorption band between 3600 and 3200 cm^{-1} was related to the O—H stretching vibrations (Fig. 4b). The sharp peak recorded at 3337 cm^{-1} might be attributed to the O—H vibrations due to intramolecular hydrogen bonding (Li & Renneckar, 2011). The absorption bands between 3000–2800 cm^{-1} and 1500–1250 cm^{-1} originated from the C—H and C—H_2 stretching and bending vibrations, respectively (Nikonenko, Buslov, Sushko, & Zhbankov, 2000; Wang & Roman, 2011). The absorption band at 1160 is related to C—O—C stretching motion. The strongest bands

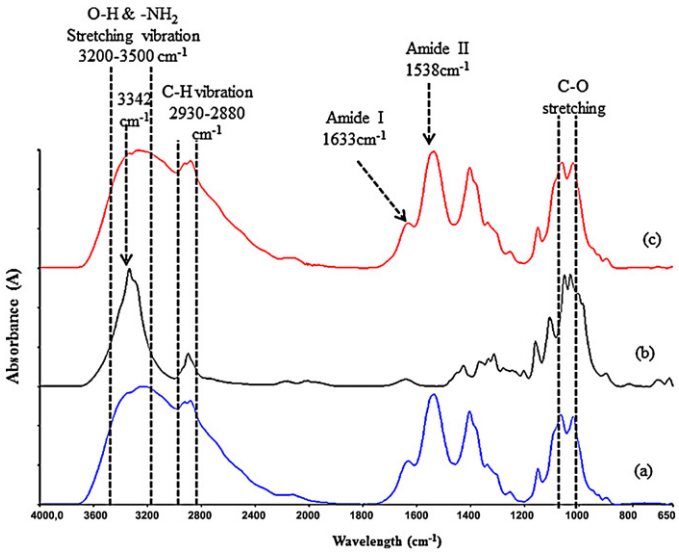

Fig. 4. FT-IR spectra of films based on (a) chitosan, (b) NCC and (c) chitosan + 5% NCC.

across NCC spectra at 1054 and 1032 cm^{-1} are assigned to C—O stretching at C-3 position. Other bands between 800 and 650 cm^{-1} originated form O—H out of plane bending vibrations (Kondo & Sawatari, 1996; Nikonenko, Buslov, Sushko, & Zhbankov, 2005). Now due to the incorporation of 5% NCC to the chitosan matrix, some differences can be observed in the FTIR spectra of chitosan films (Fig. 4c). A sharp peak appeared at 3342 cm^{-1}, which was not present in the control chitosan films. Also the intensity of the band 3342 cm^{-1} increased suggesting occurrence of hydrogen bonding between chitosan and NCC (Khan, Salmieri, et al., 2010). Other bands at 1538 and 1340 cm^{-1} had their intensity increased after NCC addition. Moreover, there was a drastic increase in the intensity of the absorption bands at 1054 and 1032 cm^{-1} due to NCC incorporation. However, other changes introduced by the addition of NCC are minor, as expected form the low amount of NCC incorporated (5%, w/w) to make the composite films.

3.5. Thermal property of the films

TGA curves for the films were represented in Fig. 5. NCC films were very stable during the heating range 50–275 °C, losing only 4.2% of its initial weight. The weight loss for the chitosan, chitosan with 5 and 10% NCC were 26.7, 27.6 and 27.8%, respectively. For all the films a major weight loss was found at around 280 °C which is

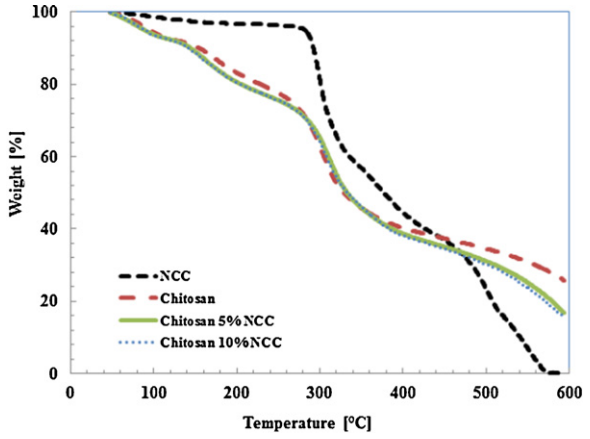

Fig. 5. TGA curves for NCC, chitosan, chitosan with 5% and 10% NCC films.

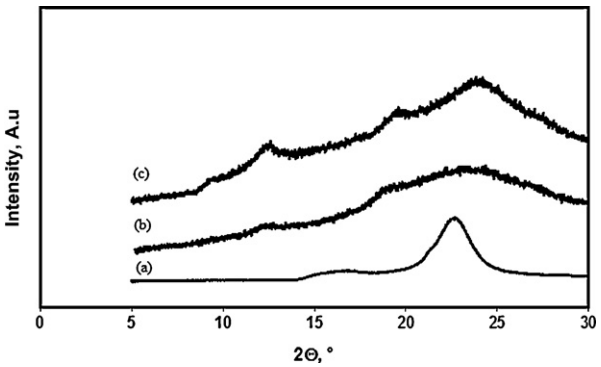

Fig. 6. X-ray diffractograms of films based on (a) NCC, (b) chitosan and (c) chitosan + 5% NCC.

associated to fast volatilization of polymer segments due to thermal scission of the polymer backbone. All chitosan samples (control, chitosan with 5% and 10% NCC films) displayed a similar thermal behavior at the temperature range 280–460 °C and the influence of NCC on the thermal stability was found to be negligible. So, apart from a small increase in the heat flow, the effect of NCC addition in the thermal property of the chitosan films was not significant.

3.6. X-ray diffraction (XRD)

Structural analysis of chitosan films and NCC containing chitosan films was investigated by XRD. Fig. 6 represents the diffractograms of the pure chitosan film and the NCC reinforced chitosan films. The diffractogram of NCC films exhibited crystalline peaks at $2\theta = 16.8°$ and 20–22.4°. The observed peaks may be due to the 1 1 0 and 2 2 0 planes of cellulose I, respectively. Shin, Gregory, and Exarhos (2007) also reported that characteristic peaks for cellulose I were in the range of $2\theta = 14.50°$, 16.65° and 22.80°. Chitosan films showed a characteristic sharp peak at around $2\theta = 13°$ and a broad halo at $2\theta = 20–23°$. The sharp peak at $2\theta = 13°$ indicated a hydrated crystalline structure, whereas the broad halo indicated an amorphous structure of chitosan (Ogawa, Hirano, Miyanishi, Yui, & Watanabe, 1994; Wang, Shen, Zhang, & Tong, 2005). Due to the incorporation of NCC into chitosan, an increase in peak intensity at $2\theta = 13°$ was observed. Also, the characteristic broad halo of amorphous chitosan at $2\theta = 20–23°$ super-positioned with the sharp peak of NCC at $2\theta = 22°$. A sharp peak at $2\theta = 25°$ was observed for the chitosan samples with 5% NCC content sample. This diffractograms suggested that NCC reinforced chitosan films exhibited a combination of amorphous and crystalline peaks (Bodin et al., 2007). The increase of peak intensity of the chitosan films may result from the transcrystallization effect. Transcrystallization can be defined as orientation of crystals of a semicrystalline matrix perpendicularly to the cellulose nanocrystals (Helbert & Chanzy, 1994). Gray (2007) reported crystallization of polymer matrix preferentially nucleated by cellulose nanocrystals, leading to a transcrystalline layer around the nanocrystals. The improvement of barrier properties of NCC-reinforced chitosan films might be attributed to the presence of crystalline regions in the films. The higher the degree of crystallinity, the lower the permeability of the films (Rhim et al., 2006). Finally, XRD supported both the mechanical and barrier properties improvement of chitosan films due to the addition of NCC.

3.7. Surface morphology of the films

Scanning electron microscopy (SEM) was employed for morphological inspection of the films. SEM reveals the homogeneity of the composite, the presence of voids, the dispersion level of the nanoparticles within the continuous matrix, the presence of

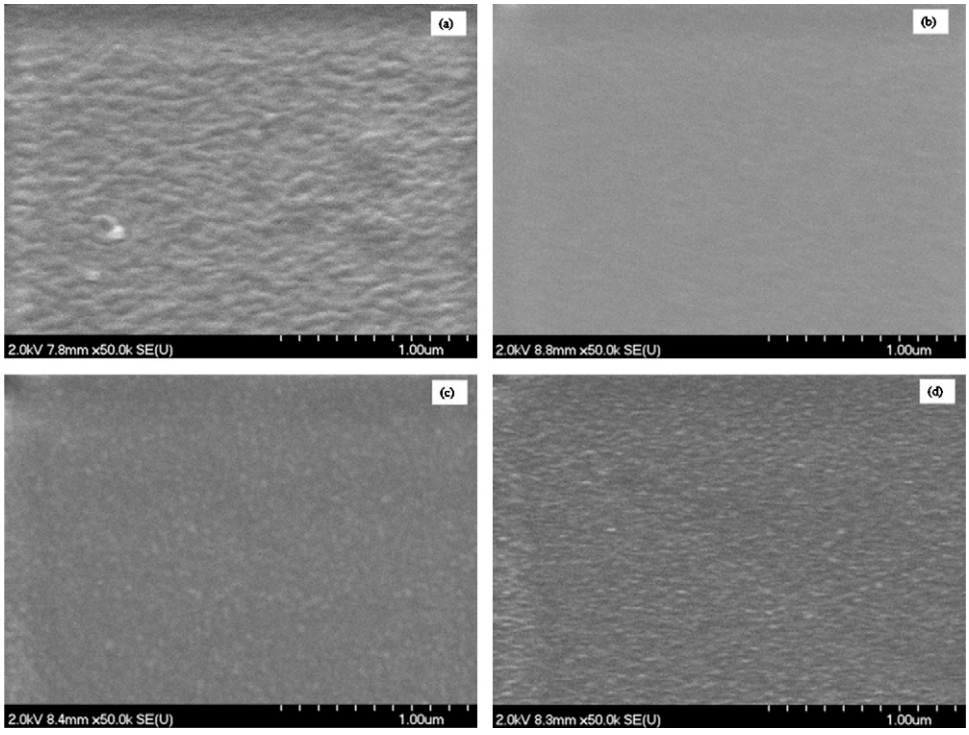

Fig. 7. SEM image of the surface of (a) NCC, (b) chitosan, (c) chitosan + 5% NCC and (d) chitosan + 10% NCC films.

aggregates and the possible orientation of nanoparticles. Fig. 7 represents SEM micrographs of the fractured surface of the (a) NCC, (b) chitosan, (c) chitosan with 5% and (d) 10% NCC films. The surface of the chitosan films (Fig. 7b) was found quite smooth which indicated better film homogenization of chitosan in aqueous media. By comparing the micrographs of chitosan (control) to that of the nanocomposite films, cellulose nanocrystals appeared like white dots in the chitosan with 5% and 10% NCC films. These shiny dots could correspond to the transversal sections of the cellulose nanocrystals (Azizi Samir, Alloin, & Dufresne, 2005). Nanocomposite films with 5% NCC content (Fig. 7c) exhibited a homogeneous and dense structure, indicating a proper dispersion of NCC into chitosan matrix. The improved mechanical properties of the nanocomposite films with 5% NCC content can be attributed

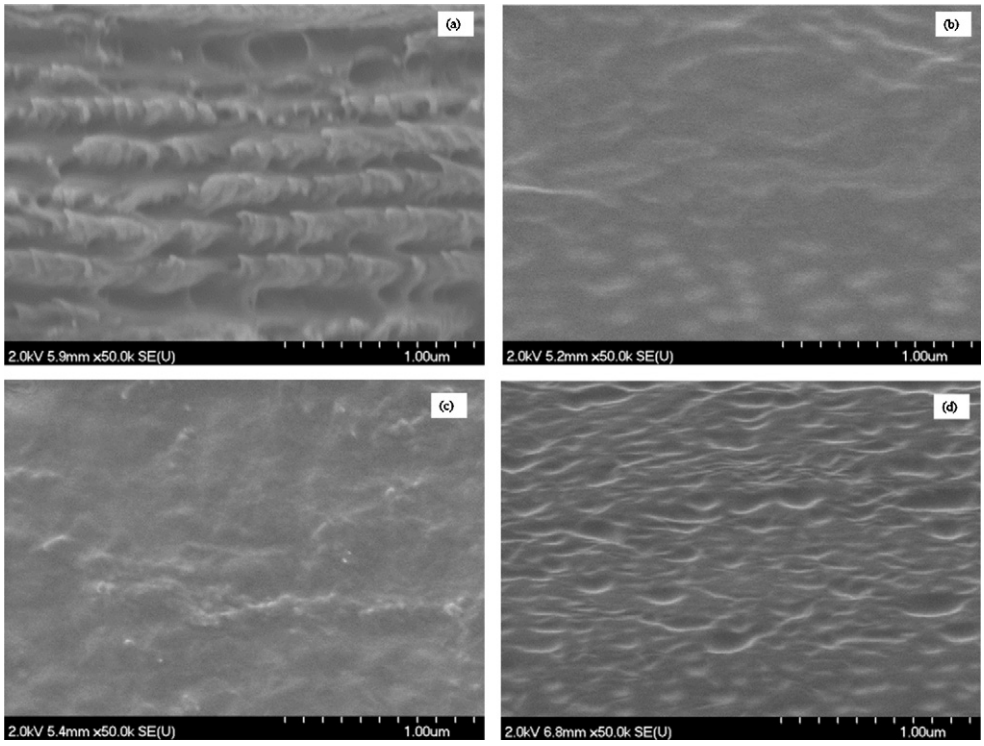

Fig. 8. SEM image of the cross-section of (a) NCC, (b) chitosan, (c) chitosan + 5% NCC and (d) chitosan + 10% NCC films.

to this homogeneous structure of the films. However, the surface became rougher with the increase in NCC content (Fig. 7d) and aggregation of NCC can be observed. An increase in the concentration of white dots was also observed. Azizi Samir et al. (2005) also reported the concentration of the white dots is a direct function of the cellulose nanocrystal composition in the composite. Fig. 8 represents SEM micrographs of the fractured cross-section of (a) NCC, (b) chitosan, (c) chitosan with 5% and (d) 10% NCC films. It is clear that addition of NCC caused changes in the film microstructure, since the non-reinforced films (Fig. 8b) exhibited a smooth surface with few cracks, as expected for a homogeneous material. Addition of 5% NCC did not affect the microstructure of the chitosan films adversely (Fig. 8c) and no bubbles or roughness appeared due to the addition of NCC. On the contrary, addition of 10% NCC (Fig. 8d) led to a rough surface, with increasing density of crack deflection sites that resulted in increasing amount of ripples and ridges as NCC concentration increased. Also, formation of some pores or bubbles (probably formed during the drying process) due to trapped air was noticed. Finally, the SEM clarifications have allowed supporting the enhanced mechanical and barrier properties of chitosan films due to the addition of NCC.

4. Conclusions

It was observed that NCC acted as a good reinforcing agent in chitosan and only 3–5% of NCC loading gave the best TS values. Improvement of the mechanical properties was due to the formation of a percolating network and strong filler–matrix interaction. Incorporation of only 5% NCC increased the TM of the chitosan films by 87%. NCC also improved the barrier properties of the chitosan by reducing the WVP and swelling property. A 27% reduction of WVP was obtained due to only 5% NCC incorporation. Surface morphology of the nanocomposite films revealed a homogeneous structure indicating proper dispersion of the NCC into the chitosan matrix. Overall, NCC reinforced nanocomposite films due to their excellent mechanical and barrier properties should have a promising impact in food packaging over the coming years.

Acknowledgements

This research was supported by the Natural Sciences and Engineering Research Council of Canada (NSERC) and by FPInnovations (Pointe-Claire, Canada) through the RDC program. The authors highly appreciate SEM support from Mrs. Line Mongeon, Technician of the Biomedical Engineering Department and the Facility Electron Microscopy Research (FEMR) at McGill University.

References

Arumugam, N., Tamareselvy, K., Venkata Rao, K., & Rajalingam, P. (1989). Coconut-fiber reinforced rubber composites. *Journal of Applied Polymer Science*, *37*, 2645–2659.

ASTM. (1999). *Standard test method for tensile strength of plastics. Annual book of ASTM standards*. ASTM International. Method D 638-99.

ASTM. (1983). *Standard test method for water vapor transmission of materials*. Philadelphia, PA: American Society for Testing & Materials. Method 15.09:E96.

Azeredo, H. M., Mattoso, L. H., Avena-Bustillos, R. J. A., Filho, G. C., Munford, M. L., Wood, D., et al. (2010). Nanocellulose reinforced chitosan composite films as affected by nanofiller loading & plasticizer content. *Journal of Food Science*, *75*, 19–28.

Azeredo, H. M. C., Mattoso, L. H. C., Wood, D., Williams, T. G., Bustillos, R. J. A., & McHugh, T. H. (2009). Nanocomposite edible films from mango puree reinforced with cellulose nanofibers. *Journal of Food Science*, *74*(5), 31–35.

Azizi Samir, M. A. S., Alloin, F., & Dufresne, A. (2005). Review of recent research into cellulosic whiskers, their properties and their application in nanocomposite field. *Biomacromolecules*, *6*(2), 612–626.

Azizi Samir, M. A. S., Alloin, F., Sanchez, J. Y., & Dufresne, A. (2004). Cellulose nanocrystals reinforced poly(oxyethylene). *Polymer*, *45*, 4149–4157.

Beck-Candanedo, S., Roman, M., & Gray, D. G. (2005). Effect of reaction conditions on the properties and behavior of wood cellulose nanocrystal suspensions. *Biomacromolecules*, *6*(2), 1048–1054.

Bodin, A., Ahrenstedt, L., Fink, H., Brumer, H., Risberg, B., & Gatenholm, P. (2007). Modification of nanocellulose with a xyloglucan–RGD conjugate enhances adhesion and proliferation of endothelial cells: Implications for tissue engineering. *Biomacromolecules*, *8*(12), 3697–3704.

Cao, X., Chen, Y., Chang, P. R., Muir, A. D., & Falk, G. (2008). Starch-based nanocomposites reinforced with flax cellulose nanocrystals. *Polymer Letters*, *2*(7), 502–510.

Cao, X., Dong, H., & Li, C. M. (2007). New nanocomposite materials reinforced with flax cellulose nanocrystals in waterborne polyurethane. *Biomacromolecules*, *8*, 899–904.

Chandra, R., & Rustgi, R. (1998). Biodegradable polymers. *Progress in Polymer Science*, *23*, 1273–1335.

Chen, M., Deng, J., Yang, F., Gong, Y., Zhao, N., & Zhang, X. (2003). Study on physical properties and nerve cell affinity of composite films from chitosan and gelatin solutions. *Biomaterials*, *24*, 2871–2880.

Ciesla, K., Salmieri, S., & Lacroix, M. (2006). γ-Irradiation influence on the structure and properties of calcium caseinate-whey protein isolate based films. Part 2: Influence of polysaccharide addition and radiation treatment on the structure and functional properties of the films. *Journal of Agricultural and Food Chemistry*, *54*, 8899–8908.

Cyras, V. P., Manfredi, L. B., Ton-That, M.-T., & Vázquez, A. (2008). Physical and mechanical properties of thermoplastic starch/montmorillonite nanocomposite films. *Carbohydrate Polymers*, *73*(1), 55–63.

Darmadji, P., & Izumimoto, M. (1994). Effect of chitosan in meat preservation. *Meat Science*, *38*(2), 243–254.

De Mesquita, J. P., Donnici, C. L., & Pereira, F. V. (2010). Biobased nanocomposites from layer-by-layer assembly of cellulose nanowhiskers with chitosan. *Biomacromolecules*, *11*(2), 473–480.

Dieter-Klemm, D., Schumann, D., Kramer, F., Hessler, N., Koth, D., & Sultanova, B. (2009). Nanocellulose materials: Different cellulose, different functionality. *Macromolecular Symposia*, *280*, 60–71.

Dong, X. M., Revol, J. F., & Gray, D. G. (1998). Effect of microcrystallite preparation conditions on the formation of colloid crystals of cellulose. *Cellulose*, *5*, 19–32.

Dufresne, A., Dupeyre, D., & Vignon, M. R. (2000). Cellulose microfibrils from potato tuber cells: Processing and characterization of starch–cellulose microfibril composites. *Journal of Applied Polymer Science*, *76*, 2080–2092.

Favier, V., Chanzy, H., & Cavaille, J. Y. (1996). Polymer nanocomposites reinforced by cellulose whiskers. *Macromolecules*, *28*, 6365–6367.

Giannelis, E. P. (1996). Polymer layered silicate nanocomposites. *Advanced Materials*, *8*(1), 29–35.

Gray, D. G. (2007). Transcrystallization of polypropylene at cellulose nanocrystal surfaces. *Cellulose*, *15*(2), 297–301.

Helbert, W., & Chanzy, H. (1994). Oriented growth of V amylase n-butanol crystals on cellulose. *Carbohydrate Polymers*, *24*, 119–122.

Jalal Uddin, A., Araki, J., & Yasuo Gotoh, Y. (2011). Toward strong green nanocomposites: Polyvinyl alcohol reinforced with extremely oriented cellulose whiskers. *Biomacromolecules*, *12*, 617–624.

Jin, J., Song, M., & Hourston, D. J. (2004). Novel chitosan-based films cross-linked by genipin with improved physical properties. *Biomacromolecules*, *5*(1), 162–168.

Jo, C., Lee, J. W., Lee, K. H., & Byun, M. W. (2001). Quality properties of pork sausage prepared with water-soluble chitosan oligomer. *Meat Science*, *59*(4), 369–375.

Kanagaraj, S., Varanda, F. R., Zhil'tsova, T. V., Oliveira, M. S. a., & Simões, J. A. O. (2007). Mechanical properties of high density polyethylene/carbon nanotube composites. *Composites Science and Technology*, *67*(15–16), 3071–3077.

Khan, A., Huq, T., Saha, M., Khan, R. A., Khan, M. A., & Gofur, M. A. (2010). Effect silane treatment on the mechanical and interfacial properties of calcium alginate fiber reinforced polypropylene composite. *Journal of Composite Materials*, *24*, 2875–2886.

Khan, R. A., Salmieri, S., Dussault, D., Calderon, J. U., Kamal, M. R., Safrany, A., et al. (2010). Production and properties of nanocellulose reinforced methylcellulose-based biodegradable films. *Journal of Agricultural and Food Chemistry*, *58*(13), 7878–7885.

Kim, K. W., Min, B. J., Kim, Y.-T., Kimmel, R. M., Cooksey, K., & Park, S. I. (2011). Antimicrobial activity against foodborne pathogens of chitosan biopolymer films of different molecular weights. *LWT – Food Science and Technology*, *44*(2), 565–569.

Kondo, T., & Sawatari, C. (1996). The assignment of IR absorption bands due to free hydroxyl groups in cellulose. *Polymer*, *37*, 393–399.

Le Tien, C., Letendre, M., Ispas-Szabo, P., Mateescu, M. A., Delmas-Patterson, G., Yu, H. L., et al. (2000). Development of biodegradable films from whey proteins by cross-linking and entrapment in cellulose. *Journal of Agricultural and Food Chemistry*, *48*, 5566–5575.

Lee, S. Y., Yang, H. S., Kim, H. J., Jeong, C. S., Lim, B. S., & Lee, J. L. (2004). Creep behavior and manufacturing parameters of wood flour filled polypropylene composites. *Composite Structures*, *65*, 459–469.

Li, Q., & Renneckar, S. (2011). Supramolecular structure characterization of molecularly thin cellulose I nanoparticles. *Biomacromolecules*, *12*, 650–659.

Li, Q., Zhou, J., & Zhang, L. (2009). Structure and properties of the nanocomposite films of chitosan reinforced with cellulose whiskers. *Journal of Polymer Science Part B: Polymer Physics*, *47*(11), 1069–1077.

Nikonenko, N. A., Buslov, D. K., Sushko, N. I., & Zhbankov, R. G. (2000). Investigation of stretching vibrations of glycosidic linkages in disaccharides and polysaccharides with use of IR spectra deconvolution. *Biopolymers*, *57*, 257–262.

Nikonenko, N. A., Buslov, D. K., Sushko, N. I., & Zhbankov, R. G. (2005). Spectroscopic manifestation of stretching vibrations of glycosidic linkage in polysaccharides. *Journal of Molecular Structure*, *752*, 20–24.

No, H. K., Meyers, S. P., Prinyawiwatkul, W., & Xu, Z. (2007). Applications of chitosan for improvement of quality and shelf life of foods: A review. *Journal of Food Science*, *72*(5), R87–R100.

Ogawa, K., Hirano, S., Miyanishi, T., Yui, T., & Watanabe, T. A. (1994). New polymorph of chitosan. *Macromolecules*, *17*, 973–975.

Paralikar, S. A., Simonsen, J., & Lombardi, J. (2008). Poly(vinyl alcohol)/cellulose nanocrystal barrier membranes. *Journal of Membrane Science*, *320*(1–2), 248–258.

Rabea, E. I., Badawy, M. E.-T., Stevens, C. V., Smagghe, G., & Steurbaut, W. (2003). Chitosan as antimicrobial agent: Applications and mode of action. *Biomacromolecules*, *4*(6), 1457–1465.

Revol, J.-F., Bradford, H., Giasson, J., Marchessault, R. H., & Gray, D. G. (1992). Helicoidal self-ordering of cellulose microfibrils in aqueous suspension. *International Journal of Biological Macromolecules*, *14*, 170–172.

Rhim, J.-W. (2011). Effect of clay contents on mechanical and water vapor barrier properties of agar-based nanocomposite films. *Carbohydrate Polymers*, *86*(2), 691–699.

Rhim, J.-W., Hong, S.-I., Park, H.-M., & Ng, P. K. W. (2006). Preparation and characterization of chitosan-based nanocomposite films with antimicrobial activity. *Journal of Agricultural and Food Chemistry*, *54*(16), 5814–5822.

Rhim, J-W., & Perry, K. W. N. G. (2007). Natural biopolymer-based nanocomposite films for packaging applications. *Critical Reviews in Food Science and Nutrition*, *47*, 411–433.

Shin, Y., Gregory, J., & Exarhos, G. J. (2007). Template synthesis of porous titania using cellulose nanocrystals. *Materials Letters*, *61*, 2594–2597.

Sionkowska, A., Wisniewski, J., Skopinska, J., Kennedy, C. J., & Wess, T. J. (2004). Molecular interactions in collagen and chitosan blends. *Biomaterials*, *25*, 795–801.

Sorrentino, A., & Gorrasi, G. (2007). Potential perspectives of bio-nanocomposites for food packaging applications. *Trends in Food Science & Technology*, *18*(2), 84–95.

Svagan, A. J., Hedenqvist, M. S., & Berglund, L. (2009). Reduced water vapour sorption in cellulose nanocomposites with starch matrix. *Composites Science and Technology*, *69*(3–4), 500–506.

Ureña-Benavides, E. E., Brown, P. J., & Kitchens, C. L. (2010). Effect of jet stretch and particle load on cellulose nanocrystal-alginate nanocomposite fibers. *Langmuir*, *26*(17), 14263–14270.

Wang, H., & Roman, M. (2011). Formation and properties of chitosan cellulose nanocrystal polyelectrolyte macroion complexes for drug delivery applications. *Biomacromolecules*, *12*, 1585–1593.

Wang, S.-F., Shen, L., Zhang, W.-D., & Tong, Y.-J. (2005). Preparation and mechanical properties of chitosan/carbon nanotubes composites. *Biomacromolecules*, *6*(6), 3067–3072.

Weber, C. J., Haugaard, V., Festersen, R., & Bertelsen, G. (2002). Production and applications of biobased packaging materials for the food industry. *Food Additives & Contaminants*, *19*, 172–177.

Wu, T., Zivanovic, S., Draughon, F. A., Conway, W. S., & Sams, C. E. (2005). Physicochemical properties and bioactivity of fungal chitin and chitosan. *Journal of Agricultural and Food Chemistry*, *53*, 3888–3894.